A Three-Region Conceptual Model for Central Pacific El Niño Including Zonal Advective Feedback

XIANG-HUI FANG AND MU MU

Department of Atmospheric and Oceanic Sciences and Institute of Atmospheric Sciences, Fudan University, Shanghai, China

(Manuscript received 22 September 2017, in final form 12 March 2018)

ABSTRACT

The simple zonal two-region framework of the recharge paradigm can accurately manifest the traditional eastern Pacific (EP) type of El Niño–Southern Oscillation (ENSO), as its major warming center is located in the EP and the anomalous sea surface temperature (SST) changes monotonically from west to east along the equatorial Pacific. However, it cannot fully depict the variations of the central Pacific (CP) type of ENSO, whose major warming center is mainly situated in the CP. Therefore, to better investigate the characteristics of the CP type of ENSO, the recharge paradigm is extended to a three-region conceptual model to describe the entire western, central, and eastern equatorial Pacific. The results show that the extended conceptual model can depict the different variations between the CP and EP well. Specifically, with increasing magnitude of the zonal advective feedback over the CP (i.e., imitating the situation for CP ENSO), the period of the system and SST magnitude over the CP and EP both decrease. However, the decreasing amplitude is more intense over the EP, indicating an enlargement of the SST differences between the CP and EP. These results are all consistent with the observational characteristics of CP ENSO.

1. Introduction

As one of the most successful conceptual models to describe the nature of El Niño–Southern Oscillation (ENSO) variability, the recharge paradigm (Jin 1997a, b) outlines many primary ENSO characteristics using its simple expression, and is widely recognized by scientists. The recharge paradigm is cast in terms of the sea surface temperature (SST) anomaly over the central to eastern part of the equatorial Pacific, where the major SST variations are located, and the thermocline depth (TCD; approximated by the depth of the 20°C isotherm) over the warm pool region of the basin. On the one hand, the TCD in the western Pacific (WP) is accompanied by the TCD over the eastern Pacific through the Sverdrup balance relationship (i.e., the balance between the zonal pressure gradient force and the zonal wind stress over the equatorial band). The TCD over the eastern Pacific amplifies the SST anomaly through the upwelling and thermocline feedback, as suggested by Bjerknes (1969). On the other hand, the TCD in the WP can lead to an ENSO-like mode based on its nonequilibrium relation with the wind stress forcing.

To explain the various conceptual models constructed previously, and to capture the main essence of the ENSO phenomenon (Bjerknes 1969; Wyrtki 1975; Zebiak and Cane 1987; Schopf and Suarez 1988; Suarez and Schopf 1988; Jin 1996), the recharge paradigm took simplification to its greatest possible extent. From the interpretation mentioned above, the main framework of the recharge paradigm is built upon a zonal two-region framework (i.e., the western and eastern equatorial Pacific). This could be correct under the hypothesis that the anomalous SST monotonically changes from west to east along the equatorial Pacific, that is, increasing (decreasing) during positive (negative) ENSO phases. In fact, this agrees well with the traditional eastern Pacific (EP) type of El Niño (Fig. 1a), with the major warming center located in the eastern Pacific region and slight cooling anomalies in the west. Since the traditional

Denotes content that is immediately available upon publication as open access.

Corresponding author: Dr. Xiang-Hui Fang, fangxh@fudan.edu.cn

DOI: 10.1175/JCLI-D-17-0633.1

EP El Niño was previously more common, and thought to be the only type of ENSO phenomenon, the recharge paradigm was widely accepted and used as an important metric to measure the ENSO simulation abilities of models at all levels of complexity.

However, since the beginning of the twenty-first century, a new type of El Niño, namely the central Pacific (CP) type (Larkin and Harrison 2005; Ashok et al. 2007; Yu and Kao 2007; Kao and Yu 2009; Kug et al. 2009), has been recognized and found to have occurred more frequently, and as such has been intensively analyzed (Yu et al. 2010; Choi et al. 2011; Newman et al. 2011; Yeh et al. 2011; Yu and Kim 2011; Chung and Li 2013; Xiang et al. 2013; Zheng et al. 2014; Fang et al. 2015; Yeh et al. 2015; Capotondi et al. 2015; Hu et al. 2016). In contrast to EP El Niño, the major warming center during CP El Niño is mainly located in the CP (Fig. 1b), with cooler SST anomalies on both sides. The figure also shows that EP El Niño is usually stronger than its CP counterpart; that is, the amplitude (maximum departure of SST from its mean state) of EP El Niño (~2.32°C) is larger than that of CP El Niño (~1.24°C). Also shown in Fig. 1 is the anomalous SST distribution during La Niña (i.e., the negative phase of ENSO). It shows that its major cooling center and amplitude (approximately −1.70°C) are both located between those of CP and EP El Niño. On the one hand, this indicates that an El Niño event is usually becoming weaker (stronger) when its major variation is located nearer the central (eastern) Pacific region. On the other hand, it highlights that since the SST anomalies during CP El Niño and La Niña do not change monotonically from west to east along the equatorial Pacific, the simple two-region recharge paradigm will not be completely suitable. In other words, the classic recharge paradigm is not capable of separating the two types of El Niño. It should be noted that although they do not vary monotonically, the anomalous SST distributions during CP El Niño and La Niña are still simple patterns of a unimodal distribution with monotonic changes on both sides of the peak area.

Different locations of the maximum SST anomalies during ENSO events also reflect the different dominant dynamics (Kug et al. 2009; Yeh et al. 2011, 2014). Physically, the anomalous warming center of EP ENSO is in the EP, where the mean thermocline is shallow enough to permit the perturbations on the subsurface to influence the SST effectively through upwelling processes, including both the thermocline feedback and Ekman feedback. In CP ENSO, the major warming center is restricted to the CP, where the thermocline is relatively deep, making the upwelling processes less effective in impacting the SST. However, since the zonal SST gradient is strongest in this region because of the warm pool to the west and the cold tongue to the east, the anomalous zonal-current-related zonal advective feedback plays a more important role. These relative contributions of the thermocline, Ekman, and zonal advective feedbacks to the development of the two types of ENSO have been widely diagnosed by observational datasets and climate model simulations (Latif 1987; Kleeman 1993; Kug et al. 2009, 2010; Capotondi 2013).

In this paper, to better describe the ENSO system and verify the impact of zonal advective feedback on CP ENSO, the recharge paradigm is extended to describe the variations over the entire western, central, and eastern equatorial Pacific. The corresponding paradigm is termed the three-region ENSO conceptual model. Following this introduction, section 2 briefly describes the data, ENSO events, and methodology used in the study. Section 3 gives a brief retrospect of the recharge paradigm. Section 4 describes the construction of a two-region ENSO conceptual model that includes zonal advective feedback. Section 5 describes the construction of the three-region ENSO conceptual model that depicts the variations over the entire western, central, and eastern equatorial Pacific. The results are summarized and discussed in section 6.

2. Datasets, ENSO event selection, and methodology

The monthly zonal wind stress, ocean temperature, and oceanic circulation data used here are all from the GODAS dataset (Behringer and Xue 2004). This dataset is available at a horizontal resolution of 1/3° × 1/3° near the tropics, and has 40 vertical levels with 10-m resolution near the surface. The analysis period is from 1980 to 2010. Anomalies presented in this study are calculated by removing the monthly mean climatology.

The methods are the same as employed in Fang et al. (2015) for the ENSO event selection, and the following text is derived from there with minor modifications. Specifically, the selection of ENSO events is based on criteria from the NOAA's operational definitions for El Niño and La Niña. Specifically, an event is defined as an El Niño (La Niña) event when the Oceanic Niño Index (ONI; the 3-month running mean of the Niño-3.4 index) is greater than or equal to 0.5°C (less than or equal to −0.5°C) for a minimum of five consecutive overlapping seasons. In addition, the type of El Niño event is determined based on the consensus method introduced by Yu et al. (2012), which consists of pattern-based and regional SST index-based methods, including the EP/CP index method of Kao and Yu (2009), the Niño method of Yeh et al. (2009), and the El Niño Modoki Index method of Ashok et al. (2007). Following this method, five events are identified as CP El Niño events: 1991/92,

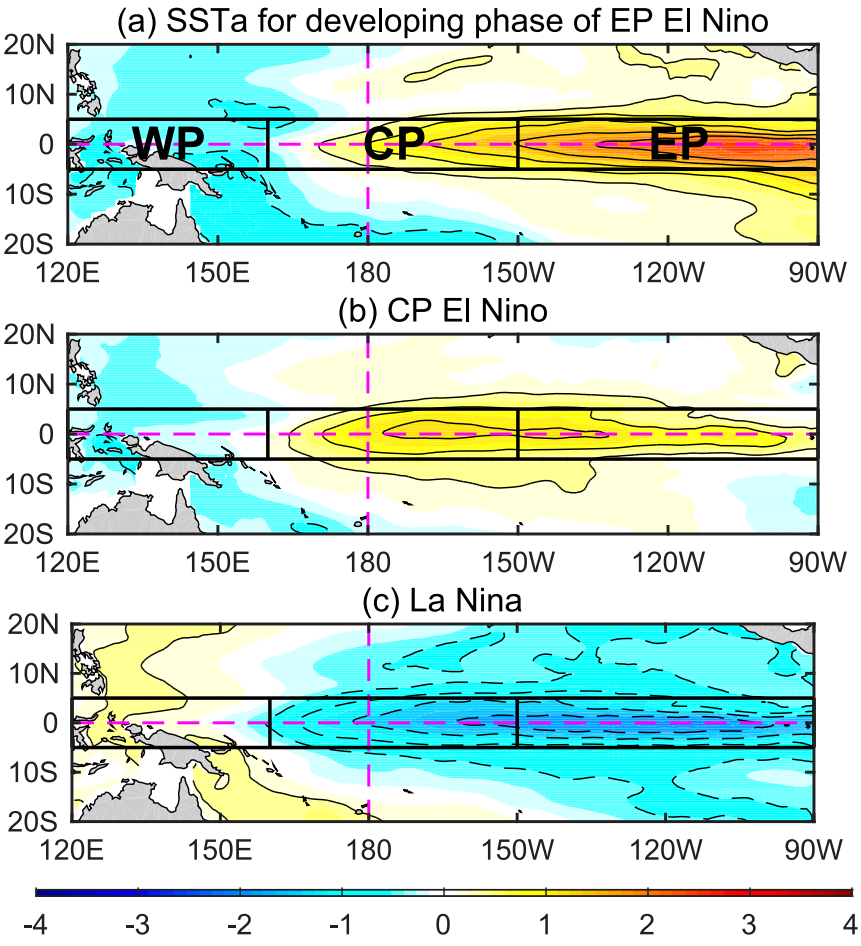

FIG. 1. Composites of SST anomalies for the developing phase of (a) EP El Niño, (b) CP El Niño, and (c) La Niña. Contour intervals are 0.4°C. Three regions in the equatorial Pacific are defined to construct the ENSO conceptual models. They are located over the western (5°S–5°N, 120°–160°E), central (5°S–5°N, 160°E–150°W), and eastern (5°S–5°N, 150°–90°W) regions of the equatorial Pacific and are termed the WP, CP, and EP, respectively.

1994/95, 2002/03, 2004/05, and 2009/10. Four events are identified as EP El Niño events: 1982/83, 1986/87, 1997/98, and 2006/07. Six events are identified as La Niña events: 1984/85, 1988/89, 1995/96, 1998/01, 2007/08, and 2010/11. For each El Niño (La Niña) event, the developing phase is defined as lasting from the month when the ONI becomes greater (less) than 0.5°C (−0.5°C) to the end of the calendar year. For example, the developing phase is from May to December for the 1982/83 El Niño event, and from August to December for the 1986/87 El Niño event.

To illustrate the differences between EP and CP types of ENSO more specifically, the EP and CP indices are first calculated based on the regression–empirical orthogonal function (EOF) method introduced by Kao and Yu (2009). Specifically, the SST anomalies regressed on the Niño-4 (5°S–5°N, 160°E–150°W) index are first subtracted from the original SST anomalies before the EOF analysis is conducted, and then the leading principal component is defined as the EP index to represent the EP ENSO variability. Similarly, the CP index is defined as the leading principal component of the SST anomalies in which the influence from the Niño-1+2 (0°–10°S, 80°–90°W) index had been subtracted.

Because data from geophysical time series are usually related to each other, the persistence and independent size of the samples must be considered when computing the statistics (Trenberth 1984; Bretherton et al. 1999). In this article, the method for calculating the degrees of freedom is identical to that used in Zheng et al. (2016), that is, the degrees of freedom can be derived using the correlation between two time series (X_i and Y_i) with different autocorrelation sequences of ρ_τ^X and ρ_τ^Y, as follows (Bretherton et al. 1999):

$$T^*_{XY} = \frac{T}{\sum_{\tau=-(T-1)}^{(T-1)}(1-|\tau|/T)\,\rho_\tau^X\,\rho_\tau^Y}, \quad (1)$$

where T^*_{XY} is the number of degrees of freedom used in the significance calculation and T is the unadjusted number of degrees of freedom.

3. A brief retrospect of the recharge paradigm

The recharge paradigm is constructed on a two-region framework over the equatorial Pacific, with a western part (5°S–5°N, 120°E–180°) and an eastern part (5°S–5°N, 180°–80°W). On the ENSO time scale, the leading ocean dynamical balance is between the zonal pressure gradient force and zonal wind stress along the equatorial Pacific (i.e., the Sverdrup balance):

$$h_E^R - h_W^R = \hat{\tau}^R, \quad (2)$$

where h_W^R and h_E^R denote the TCD anomalies in the western and eastern Pacific, respectively; $\hat{\tau}^R$ is proportional to the zonally integrated zonal wind stress along the equatorial Pacific. In the article, the superscript R of each variable denotes the recharge paradigm.

Although the thermocline tilt along the equator establishes rapidly to balance the equatorial zonal wind stress, as expressed by Eq. (2), the TCD anomalies averaged over the WP take time to adjust to the zonal integrated meridional transport (i.e., the nonequilibrium part with the wind stress forcing):

$$\frac{dh_W^R}{dt} = -rh_W^R - \alpha\hat{\tau}^R. \quad (3)$$

The first term on the right-hand side represents the ocean adjustment, which is characterized by a damping process with a rate r that collectively represents the damping of the upper ocean system, mainly through the equatorial energy loss to the boundary layer currents at the east and west sides of the ocean basin (Neelin et al. 2000). The second term represents the Sverdrup transport that is related with the zonally integrated zonal wind stress. The minus sign for the wind forcing term comes from the fact that a westerly wind stress anomaly will lead to a shallower thermocline over the WP, and vice versa.

The SST equation describes the variation over the equatorial eastern Pacific, where the local TCD is shallow and the thermocline feedback is the dominant process:

$$\frac{dT_E^R}{dt} = -cT_E^R + \gamma h_E^R, \quad (4)$$

where T_E^R is the SST anomaly averaged over the equatorial eastern Pacific and γ is the thermocline feedback coefficient. The first term on the right-hand side represents the damping process induced by the mean climatological upwelling and heat flux changes between the atmosphere and ocean.

The zonally integrated zonal wind stress anomaly is strongly coupled with the SST anomalies over the eastern equatorial Pacific, that is,

$$\hat{\tau}^R = b_0\mu T_E^R, \quad (5)$$

where b_0 is a constant that represents a high-end estimation of this air–sea coupling coefficient, and μ is a relative coupling coefficient that will vary in the range 0 to 1.5, encompassing the uncoupled and strongly coupled cases.

Combining Eqs. (2)–(5), one can obtain a simple linear coupled system with both the subsurface ocean adjustment dynamics and the surface-layer SST dynamics:

$$\begin{cases} \dfrac{dh_W^R}{dt} = -rh_W^R - \alpha b_0\mu T_E^R \\ \dfrac{dT_E^R}{dt} = rh_W^R + (-c + \gamma b_0\mu)\,T_E^R \end{cases}. \quad (6)$$

This is the main framework of the recharge paradigm, which is a two-dimensional system and is widely used to investigate the periodic essence of the ENSO system.

To facilitate quantitative analyses, one needs to estimate the values of the parameters in system (6). The collective damping rate c is dominated by the time scale over which water in the equatorial band is replaced by the mean climatological upwelling (i.e., about 2 months); γ measures the strength of the thermocline feedback, which is chosen to give an SST rate of change of 1.5 K over 2 months per 10 m of the TCD anomaly over the eastern Pacific. The collective damping rate r in the ocean adjustment is set as $(8\text{ months})^{-1}$, which is induced by the loss of energy to the boundary currents of the west and east sides of the ocean basin. Because, for a given steady zonal wind stress forcing, the zonal mean TCD anomaly of this linear system is about zero at the equilibrium state (i.e., $h_E^R + h_W^R = 0$), then from Eqs. (2) and (3) one finds that α will be about half of r; b_0, which is the high-end estimation of the thermocline tilt and is in balance with the zonal wind stress produced by the SST anomaly, is chosen to give 50 m of east–west TCD difference per 1 K of the SST anomaly. Thus, system (6) can be nondimensionalized by scales $[h] = 150$ m, $[T] = 7.5$ K, and $[t] = 2$ months for the anomalous TCD, SST, upper-layer zonal current, and the time variables, respectively. Accordingly, the parameters c, r, and α are scaled by $[t]^{-1}$, γ by $[h][t]/[T]$, and b_0 by $[T]/[h]$. Their nondimensional values are $c = 1$, $\gamma = 0.75$, $r = 0.25$, $\alpha = 0.125$, and $b_0 = 2.5$.

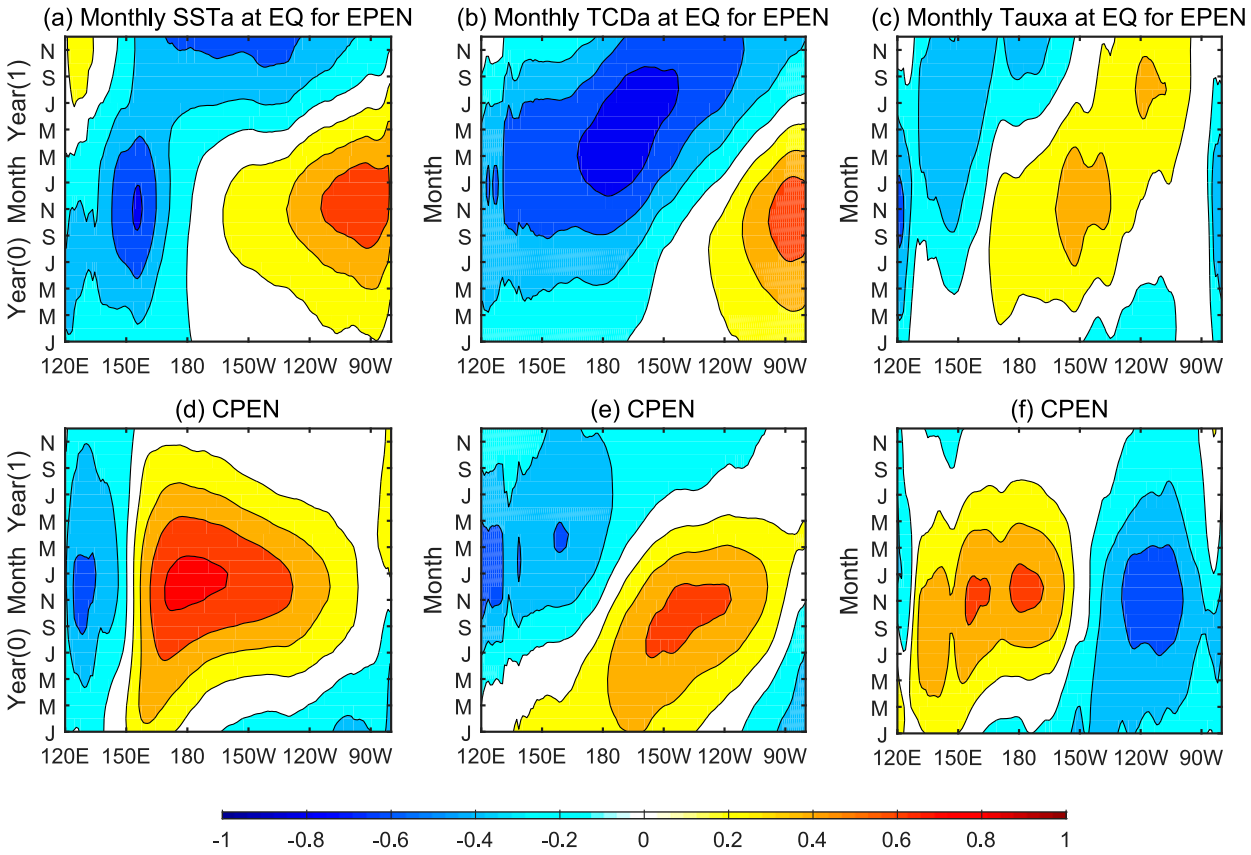

FIG. 2. Lagged correlation coefficients between the (top) EP ENSO index and (bottom) CP ENSO index and three air–sea fields along the equatorial Pacific (5°S–5°N mean). The three fields are the anomalous (a),(d) SST, (b),(e) TCD, and (c),(f) zonal wind stress (Taux). Contour intervals are 0.2. The zero lag time represents the mature phase of the ENSO events, i.e., December of the ENSO year.

4. Construction of a two-region ENSO conceptual model with zonal advective feedback

a. Feasibility of the Sverdrup balances over the western-central and central-eastern Pacific

To depict the differences in the temporal evolution of the EP and CP types of ENSO more clearly, Fig. 2 shows the lagged correlation coefficients between the EP or CP index and the SST, zonal wind stress, and TCD anomalies in the equatorial Pacific. It can be seen that, for EP El Niño, the SST anomalies show a zonal dipole pattern from west to east (Fig. 2a), which corresponds well to the assumptions of the recharge paradigm. However, during CP El Niño (Fig. 2d), the warming center is located almost entirely in the CP region (i.e., the Niño-4 region), with a lower amplitude of positive (negative) SST anomalies to the east (west). The distribution of the equatorial TCD anomalies also shows that the major positive TCD anomalies are located in the EP during EP El Niño and are closer to the CP during CP El Niño events. In agreement with the SST and TCD patterns, zonal wind stress Taux anomalies associated with CP El Niño are confined to the western Pacific, whereas they extend farther east during EP El Niño events. Based on the variations of TCD and zonal wind stress for CP (EP) type of ENSO, it may be speculated that the zonal wind stress over the central-western (central-eastern) equatorial Pacific might also be closely coupled with the corresponding thermocline slopes; in other words, the Sverdrup balance is established over the central-western (central-eastern) equatorial Pacific.

To verify these speculations, Fig. 3 shows the corresponding monthly variations of area mean zonal wind stress and the zonal gradient of TCD anomalies. Figure 3a represents the two-region recharge paradigm, in which the western part is 5°S–5°N, 120°E–180° and the eastern part is 5°S–5°N, 180°–80°W. Figure 3b represents the central-western region, in which the western part is 5°S–5°N, 120°–160°E (see WP in Fig. 1) and the central part is the Niño-4 region (see CP in Fig. 1). Figure 3c represents the central-eastern part, in which the eastern part is the Niño-3 region (see EP in Fig. 1). It can be seen that the Sverdrup balance emphasized in the recharge paradigm is indeed well satisfied, with the correlation coefficient between the two

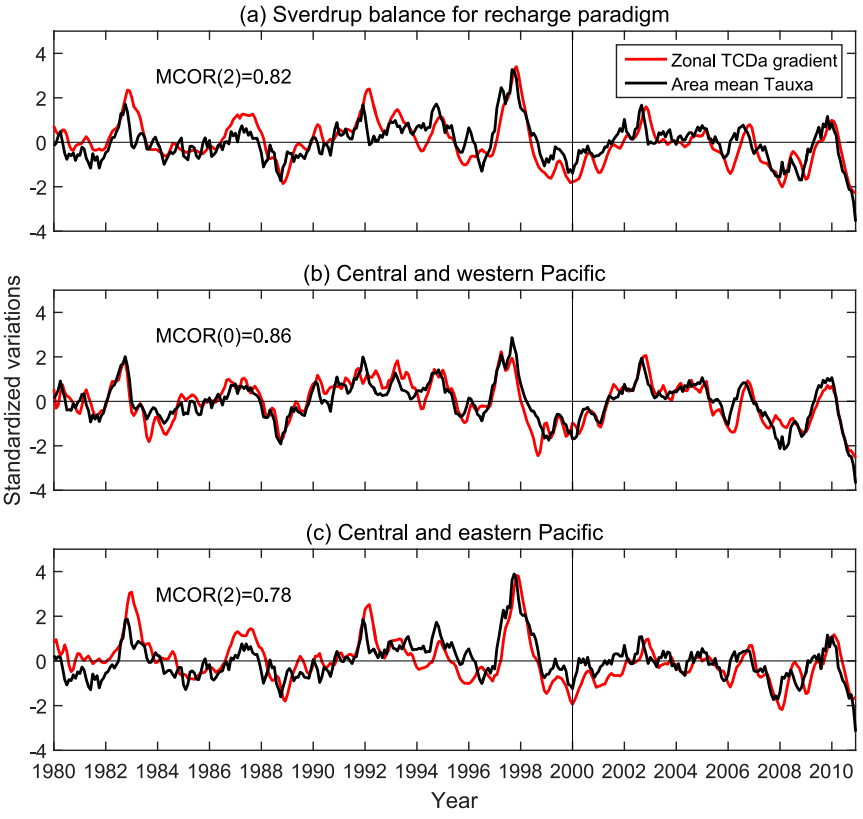

FIG. 3. Tests for the observed Sverdrup balances in different areas: (a) the recharge paradigm situation, comparing the difference between the eastern (180°–80°W) and western (120°E–180°) TCD anomalies, and the zonal wind stress averaged over the whole equatorial Pacific (120°E–80°W); (b) the central-western part, comparing the difference between the central (160°E–150°W) and western (120°–160°E) TCD anomalies, and the zonal wind stress averaged over the area 120°E–150°W; and (c) the central-eastern part, comparing the difference between the eastern (150°–90°W) and central (160°E–150°W) TCD anomalies, and the zonal wind stress averaged over the area 150°–90°W. The WP, CP, and EP are the three regions illustrated in Fig. 1. All the variations are calculated along the equator (averaged over 5°S to 5°N). The maximum correlation coefficient (MCOR) between the two variables is also shown in each panel, with the number in the bracket indicating the months that the TCD leads the zonal wind stress variable.

variables being as high as 0.75, which passes the 5% significance level with 21 degrees of freedom on the basis of the Student's *t* test. Besides, Figs. 3b and 3c indicate that the Sverdrup balances over the central-western and the central-eastern Pacific are also well satisfied, with the corresponding correlation coefficients between the area mean zonal wind stress and the corresponding zonal thermocline slope being 0.86 and 0.71, respectively. They both pass the 5% significance level on the basis of the Student's *t* test.

Owing to the fact that the warm water volume (as an index for the upper-ocean heat content averaged across the equatorial Pacific) lead time of the ENSO SST anomalies in the eastern Pacific shortens from six to seven months on average during the period 1980–99 to only a season after 2000 (McPhaden 2012), and the air–sea interaction over the equatorial Pacific changes to a state more conducive to CP El Niño after 1999 (Xiang et al. 2013), the three kinds of Sverdrup balance relationships before and after 1999 are also calculated, revealing that they are all well satisfied during both time periods (Table 1). This indicates that a two-region conceptual model over the western-central Pacific that includes zonal advective feedback, and a three-region ENSO conceptual model that depicts the entire western, central, and eastern Pacific, are both feasible to construct.

b. Constructing the conceptual model

The main difference between this two-region conceptual model and the recharge paradigm is the addition

TABLE 1. Correlation coefficients calculated for the tests of the observational Sverdrup balance in different areas. The recharge paradigm, western-central Pacific, and eastern-central Pacific correspond to the situations in Figs. 3a–c, respectively. The calculations are made for the entire period (1980–2010), and in the separate periods of 1980–99 and 2000–10.

	1980–2010	1980–99	2000–10
Recharge paradigm	0.75	0.74	0.78
Western-central Pacific	0.86	0.85	0.89
Eastern-central Pacific	0.71	0.72	0.65

of the zonal advective feedback, which is of primary importance to the development of CP ENSO. In the following work, the original framework of the recharge paradigm is retained as much as possible. On the one hand, this ensures that the new conceptual model is largely compatible with previous ENSO theories; on the other hand, it is convenient for measuring its rationality.

Since the zonal advective feedback acts as the anomalous zonal advection of the mean zonal temperature gradient, it is essential to describe the variation of the anomalous zonal current in this conceptual model. On the equatorial beta plane, the dynamic equation of the anomalous zonal current is as follows:

$$\frac{du}{dt} - \beta y v + g' \frac{\partial h}{\partial x} = -ru + \frac{\hat{\tau}}{\rho H}, \tag{7}$$

where u and v are the zonal and meridional upper-layer ocean currents, x and y are the longitude and latitude, $\hat{\tau}$ is the zonal wind stress, h is the departure of the upper-layer thickness from the reference depth H and represents the TCD anomaly, and g' is the reduced gravity parameter; r collectively represents the damping of the upper ocean system. Since the ENSO system is restricted to the equatorial region (i.e., $y \approx 0$), the beta factor on the left-hand side of Eq. (7), which manifests the influence of the rotation of Earth, can be omitted. In addition, the good Sverdrup balance relationship shown in Fig. 3b indicates that the third term on the left-hand side is well correlated with the second term on the right-hand side, so these two terms can be combined. Figure 4 shows the variations of the monthly mean zonal wind stress anomaly over the central-western Pacific and mean du/dt over the CP region, which demonstrates a robust negative relationship between these two variables. This means that the eastward wind stress anomalies along the equator will slow down the eastward zonal current. This looks unreasonable because the drag effect from the zonal wind stress to the ocean will give the zonal current a tendency to follow the wind stress. However, since the equatorial Pacific is zonally closed, the positive zonal gradient of the TCD anomaly built by the zonal wind stress (i.e., the Sverdrup balance relationship) will play a role in weakening the eastward zonal current. As a result, the variation of the zonal current is determined by the combined effect of the zonal wind stress (drag effect) and the zonal gradient of TCD anomalies (third term on the left-hand side). The calculation from Fig. 4 shows that when the zonal wind stress index leads the du/dt index by two months, the correlation coefficient between these two variables is as high as -0.45, which passes the 5% significance level with 59 degrees of freedom on the basis of the Student's t test. So, Eq. (7) can be simplified to

$$\frac{du^{2R}}{dt} = -ru^{2R} - \alpha_1 \hat{\tau}^{2R}. \tag{8}$$

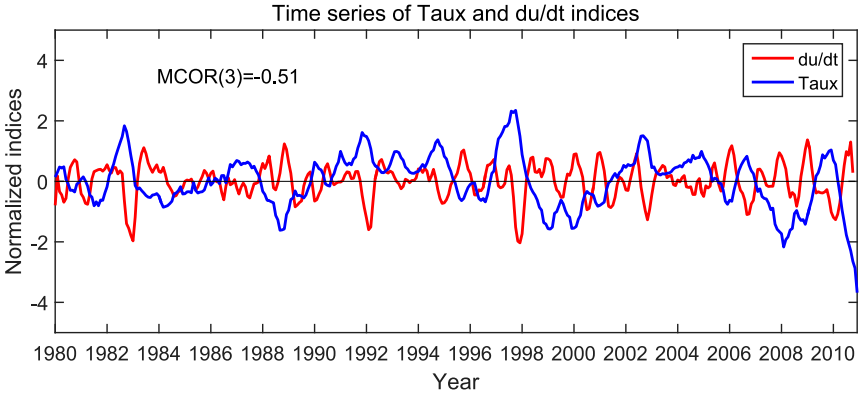

FIG. 4. The normalized indices for the zonal wind stress averaged in the central-western Pacific (5°S–5°N, 120°–160°E; blue line) and the 2-month tendency of the upper-level zonal current averaged over the CP region (red line). The maximum correlation coefficient between the two variables is also shown in the figure, with the number in the bracket indicating the months that the zonal wind stress leads the zonal current variable.

The first term on the right-hand side collectively represents the ocean damping process. The second term represents the impacts of the thermocline slope and the zonal wind stress with a combined rate α_1. The superscript $2R$ of each variable denotes the two-region conceptual model with zonal advective feedback. The Sverdrup balance gives the relationship between the zonal gradient of TCD anomalies and the area mean zonal wind stress anomalies over the central-western Pacific, that is,

$$h_C^{2R} - h_W^{2R} = \hat{\tau}^{2R}, \tag{9}$$

where h_C^{2R} and h_W^{2R} denote the area mean of the TCD anomaly over the CP and WP, respectively; $\hat{\tau}^{2R}$ denotes the area mean of the zonal wind stress anomaly over the central-western Pacific. The dynamic equation of the TCD anomaly averaged over the WP is the same as that in the recharge paradigm, that is,

$$\frac{dh_W^{2R}}{dt} = -rh_W^{2R} - \alpha_2\hat{\tau}^{2R}, \tag{10}$$

which is similar to Eq. (3), except for the central-eastern Pacific.

Through combination with Eq. (9), one can obtain the TCD anomaly averaged over the CP, which could influence the SST through the vertical advection by the mean vertical upwelling and the anomalous vertical temperature gradient (i.e., the thermocline feedback).

In contrast to the recharge paradigm, which considers the thermocline feedback as the only positive feedback over the eastern equatorial Pacific, the development of the SST over the CP is also influenced by the zonal advective feedback. Therefore, the SST equation in this region should be illustrated as follows:

$$\frac{dT_C^{2R}}{dt} = -cT_C^{2R} + \gamma h_C^{2R} + \sigma u^{2R}. \tag{11}$$

The first term on the right-hand side is the relaxation of the SST anomaly toward the climatology caused by the damping processes with a collective damping rate c. The second and third terms denote the thermocline feedback and zonal advective feedback, respectively; γ and σ are the feedback coefficients.

The simple approximate relations between the area mean zonal wind stress and SST anomalies utilized in the recharge paradigm are also retained here, that is,

$$\hat{\tau}^{2R} = b_0\mu T_C^{2R}. \tag{12}$$

Combining Eqs. (8)–(12), one can obtain a simple linear coupled system including the subsurface ocean adjustment dynamics, the surface-layer SST dynamics, and the upper-layer zonal current dynamics over the western-central Pacific regions:

$$\begin{cases} \dfrac{du^{2R}}{dt} = -ru^{2R} - \alpha_1 b_0 \mu T_C^{2R} \\ \dfrac{dT_C^{2R}}{dt} = \gamma h_W^{2R} + (-c + \gamma b_0 \mu)\, T_C^{2R} + \sigma u^{2R}. \\ \dfrac{dh_W^{2R}}{dt} = -rh_W^{2R} - \alpha_2 b_0 \mu T_C^{2R} \end{cases} \tag{13}$$

Since the zonal advective feedback is included in the SST equation, the conceptual model is extended from a two-dimensional system for the recharge paradigm to a three-dimensional linear dynamic system. It can be seen that when σ in the SST equation is set to zero (i.e., ignoring the zonal advective feedback) the system will degrade into the recharge paradigm. Thus, the system is nondimensionalized by scales of $[h] = 150\,\mathrm{m}$, $[T] = 7.5\,\mathrm{K}$, $[u] = 1.5\,\mathrm{m\,s^{-1}}$, and $[t] = 2$ months for anomalous TCD, SST, upper-layer zonal current, and the time variable, respectively. Accordingly, parameters c, r, α_1, and α_2 are scaled by $[t]^{-1}$, and parameters γ and b_0 by $[h][t]/[T]$ and $[T]/[h]$. Their nondimensional values are $c = 1$, $\gamma = 0.75$, $r = 0.25$, $\alpha_1 = 0.025$, $\alpha_2 = 0.125$, and $b_0 = 2.5$, respectively. These correspond to those used in the recharge paradigm. Note that α_1 is set to 0.025, which is 1/5 of α_2, because of the large offset between the well-related thermocline slope and zonal wind stress, as shown in Eq. (7).

With the values of the parameters given above, the dependence of the eigenmodes of the coupled system [i.e., system (13)] on the relative coupling coefficient μ can be solved analytically. As an example, Fig. 5 gives the dependence of the eigenvalues on the relative coupling coefficient when σ is set to be 4.0, in which the black and red lines are for the three kinds of growth rates and the corresponding frequencies, respectively. It shows that this three-dimensional system has a permanent damping solution that is independent from μ (i.e., the solid lines), and a pair of conjugate solutions (i.e., the dashed and circled lines that represent the oscillating solutions). Since the main purpose of this work is to investigate the essence of the oscillating phenomenon of ENSO, the contribution from the permanent damping solution will always be zero. It can be seen that when μ is small (large), the system has two decaying (amplifying) modes that are not oscillating. When μ is situated in the proper range (0.13–1.21; i.e., the air–sea coupling is not too weak or too strong), the two modes could merge into an oscillatory mode with a period mostly in the range of 2–5 years. In the following, the oscillation at the critical coupling—the relative coupling coefficient when the growth rate of the conjugate solutions is zero (e.g., 2/3 in

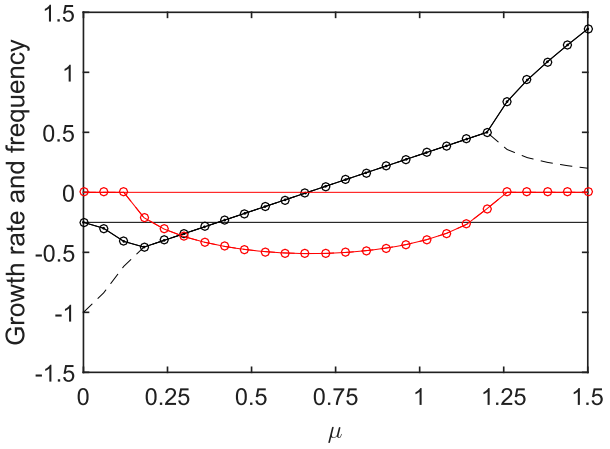

FIG. 5. Dependence of the eigenvalues on the relative coupling coefficient when σ is set to be 4.0 for system (13). The black lines show the three kinds of growth rates and the red lines show the corresponding frequencies (corresponding periods in years equal to $\pi/3$ divided by the frequencies).

Fig. 5)—is primarily analyzed to diagnose the purely oscillating phenomenon of ENSO.

To investigate the impact of the zonal advective feedback on the two-region ENSO conceptual model, Table 2 summarizes the purely oscillating solutions with different magnitudes of σ. It shows that, with increasing magnitude of zonal advective feedback, the critical coupling strength does not change, while the period and SST magnitude of the system both decrease monotonically. Specifically, when σ is zero (i.e., omitting the zonal advective feedback), the period (3.24 yr) and SST magnitude (1.47°C) are the same as those shown in the recharge paradigm. Meanwhile, when σ increases to as large as 4.0, the period and SST magnitude decrease to 2.05 years and 1.27°C, respectively. Since the zonal advective feedback becomes more important for CP ENSO, this sensitivity experiment is consistent with the characteristics reflected in Fig. 1 and the observational analysis—that is, the amplitude and period of CP ENSO are always less than those of the EP type.

5. Construction of a three-region ENSO conceptual model over the western, central, and eastern Pacific

In this section, a three-region ENSO conceptual model that depicts the air–sea interactions over the entire western, central, and eastern Pacific is constructed. The monthly variations of the thermocline slope and zonal wind stress indices over the central-western (Fig. 3b) and the central-eastern (Fig. 3c) Pacific regions indicate that the TCD anomalies over the WP, CP, and EP regions are tightly linked through the Sverdrup balance relationships. As a result, if one obtains the variation of the TCD anomalies over the WP (h_W^{3R}), those over the CP (h_C^{3R}) and EP (h_E^{3R}) can also be diagnosed. In this paper, the superscript $3R$ of each variable denotes the three-region conceptual model. Consistent with the interpretation used in the two-region conceptual model, the Sverdrup balance relationships over the central-western and the central-eastern Pacific regions are as follows:

$$\tau_1^{3R} = h_C^{3R} - h_W^{3R} = b_0\mu(T_C^{3R} + T_E^{3R})/2, \quad (14)$$

$$\tau_2^{3R} = h_E^{3R} - h_C^{3R} = b_0\mu(T_E^{3R} - T_C^{3R}), \quad (15)$$

where τ_1^{3R} and τ_2^{3R} are the area mean zonal wind stress anomalies over the central-western and the central-eastern Pacific. The right-hand sides of Eqs. (14) and (15) show the simple approximate relations between the zonal wind stress and SST anomalies; T_E^{3R} and T_C^{3R} are the mean SST anomalies over the EP and CP. It should be noted that the SST anomalies are averaged over the central-eastern Pacific but not the CP alone for the central-western Pacific subsystem [i.e., Eq. (14)]. This is consistent with the observations and corresponds to the two-region ENSO conceptual model, since the zonal wind stress over the central-western Pacific is influenced by the SST over the central-eastern Pacific but not the CP alone. Over the central-eastern Pacific [i.e., Eq. (15)], the SST anomalies are the differences between those over the CP and EP; that is, if the anomalous SST over the CP is cooler (warmer) than that over the EP, it will induce westerlies (easterlies) over the central-eastern Pacific that correspond to the local circulation. Note that the local SST anomalies (not the zonal gradient) used in the central-western Pacific subsystem exist

TABLE 2. The purely oscillating solutions with increasing influence of zonal advective feedback on SST development for system (13), in which σ denotes the strength of the zonal advective feedback on the SST development, μ_C denotes the critical coupling coefficient that makes the system exhibit a purely oscillating solution, and the T_C^{2R} magnitude is the maximum for the T_C^{2R} variable.

σ	μ	Period (yr)	T_C^{2R} magnitude (°C)
0	0.667	3.42	1.47
0.25	0.667	3.23	1.44
0.50	0.667	3.09	1.42
0.75	0.667	2.96	1.40
1.00	0.667	2.85	1.38
1.25	0.667	2.74	1.37
1.50	0.667	2.65	1.35
1.75	0.667	2.57	1.34
2.00	0.667	2.49	1.33
3.00	0.677	2.24	1.30
4.00	0.667	2.05	1.27

because the SST variation over the western Pacific region is considered to be zero.

The dynamic equations for the anomalous TCD, upper-level zonal current, and SST over the CP are the same as those in system (13). The SST equation for the EP is the same as that in the recharge paradigm, with the thermocline feedback as the only positive feedback. This means the dynamic equations for h_W^{3R}, u^{3R}, T_C^{3R}, and T_E^{3R} are as follows:

$$\frac{du^{3R}}{dt} = -ru^{3R} - \alpha_1\tau_1^{3R}, \tag{16}$$

$$\frac{dh_W^{3R}}{dt} = -rh_W^{3R} - \alpha_2\tau_1^{3R}, \tag{17}$$

$$\frac{dT_C^{3R}}{dt} = -cT_C^{3R} + \gamma h_C^{3R} + \sigma u^{3R}, \tag{18}$$

$$\frac{dT_E^{3R}}{dt} = -cT_E^{3R} + \gamma h_E^{3R}. \tag{19}$$

Combining and simplifying Eqs. (14)–(19), one can obtain a linear coupled system with four unknowns over the western, central, and eastern Pacific regions:

$$\begin{cases} \dfrac{du^{3R}}{dt} = -ru^{3R} - \dfrac{\alpha_1 b_0\mu}{2}(T_C^{3R} + T_E^{3R}) \\ \dfrac{dh_W^{3R}}{dt} = -rh_W^{3R} - \dfrac{\alpha_2 b_0\mu}{2}(T_C^{3R} + T_E^{3R}) \\ \dfrac{dT_C^{3R}}{dt} = \left(\dfrac{\gamma b_0\mu}{2} - c\right)T_C^{3R} + \dfrac{\gamma b_0\mu}{2}T_E^{3R} + \gamma h_W^{3R} + \sigma u^{3R} \\ \dfrac{dT_E^{3R}}{dt} = \gamma h_W^{3R} + \left(\dfrac{3\gamma b_0\mu}{2} - c\right)T_E^{3R} - \dfrac{\gamma b_0\mu}{2}T_C^{3R} \end{cases}. \tag{20}$$

It can be seen that when σ in Eq. (20) is set to zero (i.e., ignoring the zonal advective feedback), the system will degrade into the recharge paradigm, with $T_C^{3R} = T_E^{3R}$ and $h_C^{3R} = h_E^{3R}$, which can illustrate the EP type of ENSO with no emphasis on the differences between the CP and EP regions. Therefore, system (20) can also be seen as an extension of both the recharge paradigm and system (13). System (20) is then nondimensionalized in a similar way as for system (13), by scales of $[h] = 150\,\mathrm{m}$, $[T] = 7.5\,\mathrm{K}$, $[u] = 1.5\,\mathrm{m\,s^{-1}}$, and $[t] = 2$ months for anomalous TCD, SST, upper-layer zonal current, and the time variables, respectively. Accordingly, parameters c, r, α_1, and α_2 are scaled by $[t]^{-1}$, and parameters γ and b_0 by $[h][t]/[T]$ and $[T]/[h]$. Their nondimensional values are $c = 1$, $\gamma = 0.75$, $r = 0.25$, $\alpha_1 = 0.025$, $\alpha_2 = 0.125$, and $b_0 = 2.5$, which all correspond to those used in the recharge paradigm and system (13). Analytically, this four-dimensional system also has a pair of conjugate solutions (i.e., oscillating solutions). As an example, Fig. 6 shows the dependence of the eigenvalues on the relative coupling coefficient when σ is set to be 0.25, in which the black and red lines are for the four kinds of growth rates and the corresponding frequencies, respectively. It can be seen that a pair of conjugate solutions (i.e., the lines with circle and plus sign that represent the oscillating solutions), with a period mostly in the range of 2–5 years, exists when μ is situated in a proper range (i.e., 0.20–0.93). Similarly, since the main purpose of this work is to investigate the essence of the oscillating phenomenon of ENSO, the contribution from the other two solutions, a permanent damping one (solid lines) and a nonoscillating one (dashed lines), will always be zero.

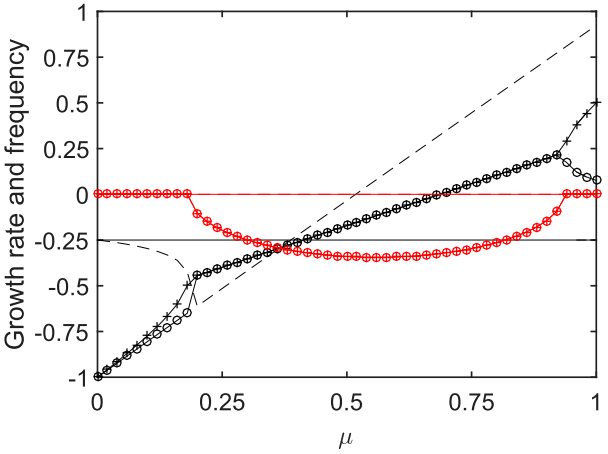

FIG. 6. Dependence of the eigenvalues on the relative coupling coefficient when σ is set to be 0.25 for system (20). The black curves show the four kinds of growth rates and the red curves show the corresponding frequencies (corresponding periods in years equal to $\pi/3$ divided by the frequencies).

Table 3 gives the purely oscillating solutions with different magnitudes of zonal advective feedback for the SST development over the CP region. Similar to the results from system (13), it shows that with increasing magnitude of zonal advective feedback the ENSO period and SST magnitudes over the central and eastern Pacific both decrease. However, the decrement is more intense over the EP, indicating an enlargement of the SST differences between the CP and EP. Since the zonal advective feedback plays a more important role in the SST development over the CP for CP El Niño, this could explain the weaker amplitude and shorter period of CP ENSO. It should be noted that, although the critical coupling strength (μ_C) increases with increasing magnitude of zonal advective feedback, the variation of the zonal wind stress over the western-central Pacific [τ_1^{3R}, which is the product of $(T_C^{3R} + T_E^{3R})/2$ and μ_C] is still decreasing, indicating a comprehensive weakening of the ENSO system. Furthermore, the magnitude of the

TABLE 3. The purely oscillating solutions with increasing influence of zonal advective feedback on SST development for system (20), in which σ denotes the strength of the zonal advective feedback on the SST development, μ_C denotes the critical coupling coefficient that makes the system exhibit a purely oscillating solution, and the magnitudes for τ_1^{3R}, T_C^{3R}, T_E^{3R}, and h_m^{3E} are the maximums for the variables, respectively.

σ	μ_C	τ_1^{3R} magnitude (N m^{-2})	Period (yr)	T_C^{3R} magnitude (°C)	T_E^{3R} magnitude (°C)	h_m^{3E} magnitude (m)
0	0.667	34.56	3.42	1.449	1.449	13.31
0.25	0.686	34.25	3.23	1.423	1.339	13.19
0.50	0.702	33.61	3.06	1.397	1.251	12.64
0.75	0.715	32.54	2.90	1.379	1.184	12.55
1.00	0.727	32.82	2.77	1.359	1.128	12.53
1.25	0.737	32.39	2.65	1.346	1.082	12.18
1.50	0.746	31.64	2.54	1.336	1.043	12.16
1.75	0.754	31.79	2.45	1.327	1.009	12.20
2.00	0.762	31.61	2.37	1.317	0.980	11.95
3.00	0.789	30.97	2.10	1.291	0.892	11.68
4.00	0.810	30.59	1.91	1.270	0.832	11.52

zonal mean TCD anomalies along the equator (h_m^{3E}), which could partly measure the magnitude of water exchange between the equatorial and extra-equatorial Pacific, also decreases consistently in this system, albeit with unexpected increases from $\sigma = 1.50$ to $\sigma = 1.75$. This result is consistent with the observational analyses reported by Kug et al. (2009), in which the evolution of the zonal mean sea level anomalies over the Pacific basin was used to examine the heat exchange between the equatorial and extra-equatorial Pacific regions. Their results indicated that the recharge oscillator theory holds well for EP ENSO, in which the positive anomaly of equatorial heat content leads El Niño by about a quarter cycle of the ENSO period, and the heat content anomaly is efficiently discharged after the peak phase of El Niño. However, the transport of equatorial heat content is quite weak during the decaying phase of CP El Niño, indicating a weak recharge–discharge process. This also indicates that the recharge oscillator theory cannot fully explain the phenomenon of CP ENSO.

Two examples of the solution for system (20) are shown in Figs. 7a and 7b, with σ being 0.25 and 4.00, respectively. It can be seen that when σ is 0.25 (i.e., relatively weak zonal advective feedback), the variations over the central and eastern Pacific are almost the same. Also, the period of system (20) in this situation is 3.23 years, and the SST magnitude over the CP is about 1.423°C. However, when σ is 4.00 (i.e., relatively strong zonal advective feedback), large differences exist between the CP and EP. This shows that the variations of both the SST and TCD anomalies over the CP are more intense than those over the EP. The period of system (20) in this situation shortens to 1.91 years, and the SST magnitudes over the CP and EP are about 1.27° and

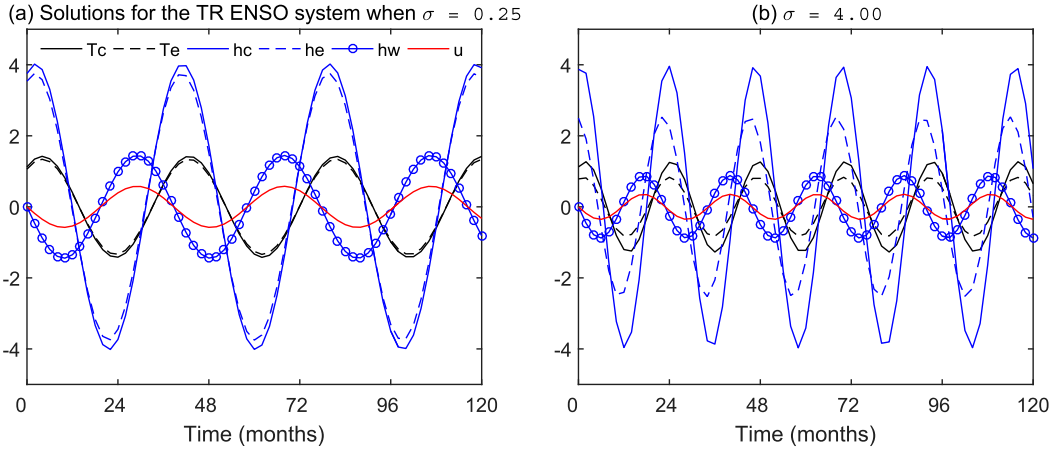

FIG. 7. Time series of the anomalous SST (in °C) over the CP (solid black line) and EP (dashed black line); TCD (in 10 m) over the western (circled blue line), central (solid blue line), and eastern Pacific (dashed blue line); and zonal current (in 0.05 m s^{-1}) over the CP (red line) of the solution from system (20) with σ equal to (a) 0.25 and (b) 4.00. The initial condition for the SST over the CP is 1.125°C, and for the TCD over the WP it is 0 m.

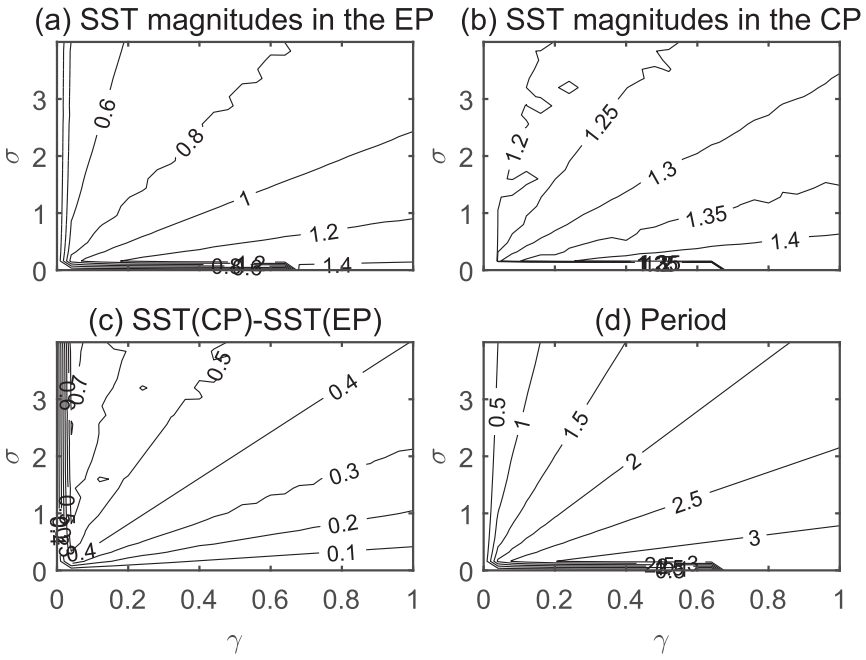

FIG. 8. Characteristics of the purely oscillating solutions with different amplitudes of γ and σ for system (20): (a) SST magnitudes in the EP region (in °C), (b) SST magnitudes in the CP region (in °C), (c) SST magnitude differences between the CP and EP (in °C), and (d) period (in yr).

0.832°C, respectively. This depicts the pattern shown in the observational CP ENSO reasonably well, in which the major warming center is located almost entirely in the CP, with cooler SST anomalies on both sides. These results indicate that constructing a three-region ENSO conceptual model over the equatorial Pacific can better describe the ENSO system when considering the zonal advective feedback to the development of SSTs over the CP, and is more able to depict the differences between the two types of ENSO.

A double sensitivity experiment with respect to both the zonal advective and thermocline feedback amplitudes (i.e., σ and γ) is performed to investigate system (20). The results are shown in Fig. 8, in which the main characteristics of the corresponding purely oscillating solutions are presented. It can be seen that the system is sensitive to both feedbacks. When γ is constant (i.e., a constant thermocline feedback), the period of the system and the main SST magnitude in the central-eastern Pacific are decreasing with the increasing magnitude of the zonal advective feedback (i.e., σ). These results are consistent with those shown in the single sensitivity experiment for σ (i.e., Table 3). In addition, when the zonal advective feedback is constant, the period of the system and the main SST magnitude in the central-eastern Pacific are increasing with the increasing magnitude of the thermocline feedback. However, the increment is more intense over the EP, indicating a reduction in the SST differences between the CP and EP. This result is consistent with the observational analyses reported by Hu et al. (2013) and Lübbecke and McPhaden (2014), who argued that the thermocline feedback in the central-eastern Pacific is reduced from 1980–98 to 1999–2010, which leads to the weaker amplitude of ENSO during 1999–2010 and favors the occurrence of CP El Niño.

6. Summary and discussion

The classical ENSO conceptual model, the recharge paradigm, outlines many primary ENSO characteristics via its simple expression. The model was cast in terms of the SST anomaly over the central to eastern part of the equatorial Pacific and the TCD over the warm pool region of the basin (i.e., a two-region conceptual model). However, since the beginning of the twenty-first century, the CP El Niño, whose major warming center is mainly focused in the CP, has occurred more frequently. Furthermore, La Niña also shows a pattern whereby the major cooling center and amplitude are both located between the CP and EP El Niño types. This indicates that the simple east–west, two-region recharge paradigm is not very suitable for CP El Niño and La Niña. Therefore, to better describe the ENSO system and

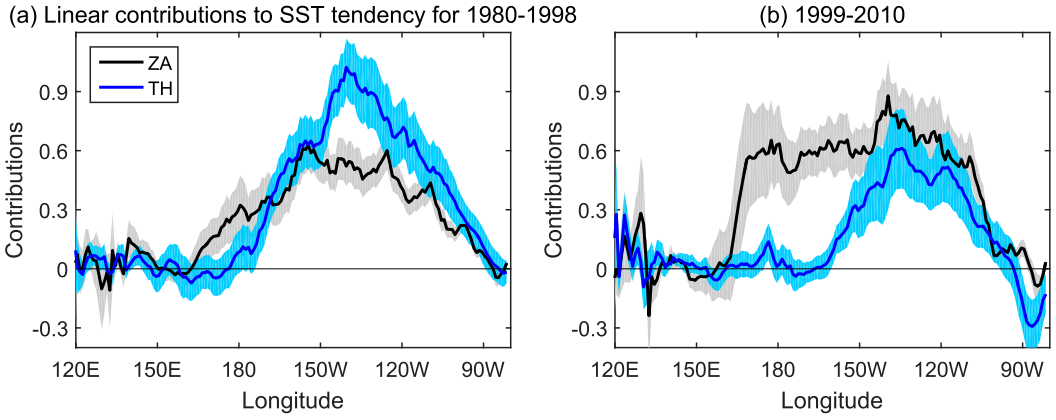

FIG. 9. Observational linear contributions of zonal advective feedback (ZA; black line and gray shading) and thermocline feedback (TH; blue line and shading) to the SST tendency across the equatorial Pacific during (a) 1980–98 and (b) 1999–2010. The shaded regions indicate the 95% confidence values from the Student's *t* test.

investigate the differences between the two types of ENSO, the recharge paradigm is extended in the present study to depict the entire western, central, and eastern equatorial Pacific, and is termed the three-region ENSO conceptual model.

First, a two-region conceptual model is constructed to add the zonal advective feedback, which has been widely reported to play a primary role in CP El Niño but was not included in the recharge paradigm. Since the zonal advective feedback is the anomalous zonal advection of the mean zonal temperature gradient, one needs to introduce the dynamic equation of the upper-layer zonal current. As a result, a three-dimensional dynamic system [i.e., system (13)] is obtained. The sensitivity experiments indicate that, with increasing magnitude of zonal advective feedback to SST development, the period and SST magnitude both decrease. Since the zonal advective feedback becomes more important for CP El Niño, these sensitivity experiments are consistent with the fact that the amplitude and period of CP ENSO are usually less than those of the EP type.

Next, a three-region ENSO conceptual model, which depicts the variations over the western, central, and eastern Pacific simultaneously, is constructed (section 5). This gives a four-dimensional system [i.e., system (20)], which is an extension of both the recharge paradigm and system (13). The zonal advective feedback strength sensitivity experiments are repeated for system (20). The primary results are similar to those for system (13); that is, with increasing magnitude of zonal advective feedback to SST development over the CP, the ENSO period and SST magnitude over the central and eastern Pacific both decrease. However, the decreasing amplitude is more intense over the EP, indicating an enlargement of the SST differences between the CP and EP. Also, the variability of the zonal mean TCD anomalies along the equator, which could partly reflect the magnitude of water exchange between the equatorial and extra-equatorial Pacific, shows a consistent decrement with increasing magnitude of zonal advective feedback. This is consistent with the observational analysis of Kug et al. (2009), in which the evolution of the zonal mean sea level anomalies over the Pacific basin was used to examine the heat exchange between the equatorial and extra-equatorial Pacific regions. Their results indicated that the recharge oscillator theory holds well for EP El Niño. However, the transport of equatorial heat content is quite weak during the decaying phase of CP El Niño; that is, there is a weak recharge–discharge process.

A double sensitivity experiment with respect to both the zonal advective and thermocline feedback amplitudes is also performed to investigate the three-region ENSO conceptual model. The results indicate that the system is sensitive to both feedbacks. Different from the role played by the zonal advective feedback, with the increasing magnitude of the thermocline feedback, the period of the system and the SST magnitude in the central-eastern Pacific all increase. Because the increment is more intense over the EP, the differences between the CP and EP reduce.

It has been documented that CP El Niño has occurred more frequently in the last decade. Xiang et al. (2013) argued that the background state changes (i.e., a La Niña–like pattern) observed in the tropical Pacific around the late 1990s may favor the occurrence of CP El Niño through suppressing convection and low-level convergence in the CP. Hu et al. (2013) and Lübbecke and McPhaden (2014) also argued that the thermocline feedback in the central-eastern Pacific is reduced from

1980–98 to 1999–2010, which leads to the weaker amplitude of ENSO during 1999–2010 and favors the occurrence of CP El Niño. Within the framework of the three-region ENSO conceptual model, this can be easily understood. Based on the budget analysis method introduced by Kug et al. (2009), the observed linear contributions of zonal advective feedback and thermocline feedback to the SST tendency along the equatorial Pacific during the periods 1980–98 and 1999–2010 are calculated (Fig. 9). It can be seen that, during the earlier decade, when EP ENSO is more common, the thermocline feedback plays the dominant role over the central-eastern Pacific region. However, during the most recent decade, the zonal advective feedback over the CP strengthens, while the thermocline feedback over the central-eastern Pacific weakens. This has led to a more dominant role played by zonal advective feedback in the ENSO system. When we calculate the nondimensionalized parameters σ (in the CP) and γ (in the central-eastern Pacific), it is found that they are 0.48 and 0.86 during 1980–98, whereas they are 0.56 and 0.35 during 1999–2010. This means the zonal advective feedback (thermocline feedback) is increasing (decreasing) from 1980–98 to 1999–2010. As shown in Fig. 8, these two changes both favor the occurrence of the CP type of ENSO.

Based on the three-region ENSO conceptual model, the different characteristics between the CP and EP types of ENSO can be investigated. However, because of its linearity and simplicity, it cannot currently manifest the two types of ENSO within one framework. Nevertheless, this could be achieved in the future by introducing other physical processes and stochastic terms. In addition, the nonlinearity of the ENSO system (e.g., the asymmetry between the positive and negative phases of ENSO) is another important issue that should be investigated in the model.

Acknowledgments. This work was supported by the Project funded by China Postdoctoral Science Foundation (Grant 2017M610225). The observational monthly data were all obtained from the website http://www.cpc.ncep.noaa.gov/products/GODAS/.

REFERENCES

Ashok, K., S. K. Behera, S. A. Rao, H. Weng, and T. Yamagata, 2007: El Niño Modoki and its possible teleconnection. *J. Geophys. Res.*, **112**, C11007, https://doi.org/10.1029/2006JC003798.

Behringer, D., and Y. Xue, 2004: Evaluation of the global ocean data assimilation system at NCEP: The Pacific Ocean. *Eighth Symp. on Integrated Observing and Assimilation Systems for Atmosphere, Oceans, and Land Surface*, Seattle, WA, Amer. Meteor. Soc., 2.3, https://ams.confex.com/ams/pdfpapers/70720.pdf.

Bjerknes, J., 1969: Atmospheric teleconnections from the equatorial Pacific. *Mon. Wea. Rev.*, **97**, 163–172, https://doi.org/10.1175/1520-0493(1969)097<0163:ATFTEP>2.3.CO;2.

Bretherton, C. S., M. Widmann, V. P. Dymnikov, J. M. Wallace, and I. Bladé, 1999: The effective number of spatial degrees of freedom of a time-varying field. *J. Climate*, **12**, 1990–2009, https://doi.org/10.1175/1520-0442(1999)012<1990:TENOSD>2.0.CO;2.

Capotondi, A., 2013: ENSO diversity in the NCAR CCSM4 climate model. *J. Geophys. Res. Oceans*, **118**, 4755–4770, https://doi.org/10.1002/jgrc.20335.

——, and Coauthors, 2015: Understanding ENSO diversity. *Bull. Amer. Meteor. Soc.*, **96**, 921–938, https://doi.org/10.1175/BAMS-D-13-00117.1.

Choi, J., S. -I. An, J. -S. Kug, and S. -W. Yeh, 2011: The role of mean state on changes in El Niño's flavor. *Climate Dyn.*, **37**, 1205–1215, https://doi.org/10.1007/s00382-010-0912-1.

Chung, P. -H., and T. Li, 2013: Interdecadal relationship between the mean state and El Niño types. *J. Climate*, **26**, 361–379, https://doi.org/10.1175/JCLI-D-12-00106.1.

Fang, X.-H., F. Zheng, and J. Zhu, 2015: The cloud-radiative effect when simulating strength asymmetry in two types of El Niño events using CMIP5 models. *J. Geophys. Res. Oceans*, **120**, 4357–4369, https://doi.org/10.1002/2014JC010683.

Hu, C., S. Yang, Q. Wu, T. Zhang, C. Zhang, Y. Li, K. Deng, T. Wang, and J. Chen, 2016: Reinspecting two types of El Niño: A new pair of Niño indices for improving real-time ENSO monitoring. *Climate Dyn.*, **47**, 4031–4049, https://doi.org/10.1007/s00382-016-3059-x.

Hu, Z.-Z., A. Kumar, H.-L. Ren, H. Wang, M. L'Heureux, and F.-F. Jin, 2013: Weakened interannual variability in the tropical Pacific Ocean since 2000. *J. Climate*, **26**, 2601–2613, https://doi.org/10.1175/JCLI-D-12-00265.1.

Jin, F.-F., 1996: Tropical ocean–atmosphere interaction, the Pacific cold tongue, and the El Niño–Southern Oscillation. *Science*, **274**, 76–78, https://doi.org/10.1126/science.274.5284.76.

——, 1997a: An equatorial ocean recharge paradigm for ENSO. Part I: Conceptual model. *J. Atmos. Sci.*, **54**, 811–829, https://doi.org/10.1175/1520-0469(1997)054<0811:AEORPF>2.0.CO;2.

——, 1997b: An equatorial ocean recharge paradigm for ENSO. Part II: A stripped-down coupled model. *J. Atmos. Sci.*, **54**, 830–847, https://doi.org/10.1175/1520-0469(1997)054<0830:AEORPF>2.0.CO;2.

Kao, H. -Y., and J.-Y. Yu, 2009: Contrasting eastern-Pacific and central-Pacific types of ENSO. *J. Climate*, **22**, 615–632, https://doi.org/10.1175/2008JCLI2309.1.

Kleeman, R., 1993: On the dependence of hindcast skill on ocean thermodynamics in a coupled ocean–atmosphere model. *J. Climate*, **6**, 2012–2033, https://doi.org/10.1175/1520-0442(1993)006<2012:OTDOHS>2.0.CO;2.

Kug, J.-S., F.-F. Jin, and S.-I. An, 2009: Two types of El Niño events: Cold tongue El Niño and warm pool El Niño. *J. Climate*, **22**, 1499–1515, https://doi.org/10.1175/2008JCLI2624.1.

——, J. Choi, S.-I. An, F.-F. Jin, and A. T. Wittenberg, 2010: Warm pool and cold tongue El Niño events as simulated by the GFDL 2.1 coupled GCM. *J. Climate*, **23**, 1226–1239, https://doi.org/10.1175/2009JCLI3293.1.

Larkin, N. K., and D. E. Harrison, 2005: Global seasonal temperature and precipitation anomalies during El Niño autumn and winter. *Geophys. Res. Lett.*, **32**, L16705, https://doi.org/10.1029/2005GL022860.

Latif, M., 1987: Tropical ocean circulation experiments. *J. Phys. Oceanogr.*, **17**, 246–263, https://doi.org/10.1175/1520-0485(1987)017<0246:TOCE>2.0.CO;2.

Lübbecke, J. F., and M. J. McPhaden, 2014: Assessing the twenty-first-century shift in ENSO variability in terms of the Bjerknes stability index. *J. Climate*, **27**, 2577–2587, https://doi.org/10.1175/JCLI-D-13-00438.1.

McPhaden, M. J., 2012: A 21st century shift in the relationship between ENSO SST and warm water volume anomalies. *Geophys. Res. Lett.*, **39**, L09706, https://doi.org/10.1029/2012GL051826.

Neelin, J. D., F.-F. Jin, and H.-H. Syu, 2000: Variations in ENSO phase locking. *J. Climate*, **13**, 2570–2590, https://doi.org/10.1175/1520-0442(2000)013<2570:VIEPL>2.0.CO;2.

Newman, M., S. -I. Shin, and M. A. Alexander, 2011: Natural variation in ENSO flavors. *Geophys. Res. Lett.*, **38**, L14705, https://doi.org/10.1029/2011GL047658.

Schopf, P. S., and M. J. Suarez, 1988: Vacillations in a coupled ocean–atmosphere model. *J. Atmos. Sci.*, **45**, 549–566, https://doi.org/10.1175/1520-0469(1988)045<0549:VIACOM>2.0.CO;2.

Suarez, M. J., and P. S. Schopf, 1988: A delayed action oscillator for ENSO. *J. Atmos. Sci.*, **45**, 3283–3287, https://doi.org/10.1175/1520-0469(1988)045<3283:ADAOFE>2.0.CO;2.

Trenberth, K. E., 1984: Some effects of finite sample size and persistence on meteorological statistics. Part I: autocorrelations. *Mon. Wea. Rev.*, **112**, 2359–2368, https://doi.org/10.1175/1520-0493(1984)112<2359:SEOFSS>2.0.CO;2.

Wyrtki, K., 1975: El Niño—The dynamic response of the equatorial Pacific Ocean to atmospheric forcing. *J. Phys. Oceanogr.*, **5**, 572–584, https://doi.org/10.1175/1520-0485(1975)005<0572:ENTDRO>2.0.CO;2.

Xiang, B., B. Wang, and T. Li, 2013: A new paradigm for predominance of standing central Pacific warming after the late 1990s. *Climate Dyn.*, **41**, 327–340, https://doi.org/10.1007/s00382-012-1427-8.

Yeh, S.-W., J.-S. Kug, B. Dewitte, M.-H. Kwon, B. P. Kirtman, and F.-F. Jin, 2009: El Niño in a changing climate. *Nature*, **461**, 511–515, https://doi.org/10.1038/nature08316.

——, B. P. Kirtman, J. -S. Kug, W. Park, and M. Latif, 2011: Natural variability of the central Pacific El Niño event on multi-centennial timescales. *Geophys. Res. Lett.*, **38**, L02704, https://doi.org/10.1029/2010GL045886.

——, J.-S. Kug, and S.-I. An, 2014: Recent progress on two types of El Niño: Observations, dynamics, and future changes. *Asia-Pac. J. Atmos. Sci.*, **50**, 69–81, https://doi.org/10.1007/s13143-014-0028-3.

——, X. Wang, C. Wang, and B. Dewitte, 2015: On the relationship between the North Pacific climate variability and the central Pacific El Niño. *J. Climate*, **28**, 663–677, https://doi.org/10.1175/JCLI-D-14-00137.1.

Yu, J.-Y., and H.-Y. Kao, 2007: Decadal changes of ENSO persistence barrier in SST and ocean heat content indices: 1958–2001. *J. Geophys. Res.*, **112**, D13106, https://doi.org/10.1029/2006JD007654.

——, and S.-T. Kim, 2011: Relationships between extratropical sea level pressure variations and the central Pacific and eastern Pacific types of ENSO. *J. Climate*, **24**, 708–720, https://doi.org/10.1175/2010JCLI3688.1.

——, H.-Y. Kao, and T. Lee, 2010: Subtropics-related interannual sea surface temperature variability in the central equatorial Pacific. *J. Climate*, **23**, 2869–2884, https://doi.org/10.1175/2010JCLI3171.1.

——, Y. Zou, S.-T. Kim, and T. Lee, 2012: The changing impact of El Niño on US winter temperatures. *Geophys. Res. Lett.*, **39**, L15702, https://doi.org/10.1029/2012GL052483.

Zebiak, S. E., and M. A. Cane, 1987: A model El Niño–Southern Oscillation. *Mon. Wea. Rev.*, **115**, 2262–2278, https://doi.org/10.1175/1520-0493(1987)115<2262:AMENO>2.0.CO;2.

Zheng, F., X.-H. Fang, J.-Y. Yu, and J. Zhu, 2014: Asymmetry of the Bjerknes positive feedback between the two types of El Niño. *Geophys. Res. Lett.*, **41**, 7651–7657, https://doi.org/10.1002/2014GL062125.

——, ——, J. Zhu, J.-Y. Yu, and X.-C. Li, 2016: Modulation of Bjerknes feedback on the decadal variations in ENSO predictability. *Geophys. Res. Lett.*, **43**, 12 560–12 568, https://doi.org/10.1002/2016GL071636.